

Vibrational Properties and Specific Heat of Ultrananocrystalline Diamond: Molecular Dynamics Simulations

Shashishekhar P. Adiga,^{*†} Vivekananda P. Adiga,[‡] Robert W. Carpick,[§] and Donald W. Brenner^{||}

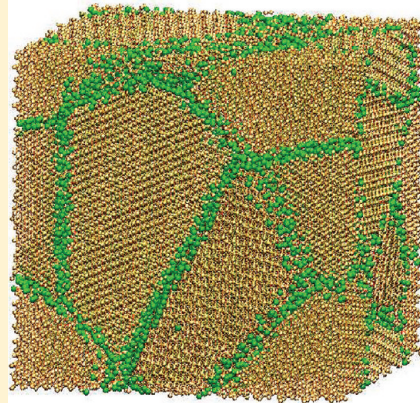
[†]Kodak Research Laboratories, Eastman Kodak Company, Rochester, New York 14620, United States

[‡]School of Applied and Engineering Physics, Cornell University, Ithaca, New York 14853, United States

[§]Department of Mechanical Engineering and Applied Mechanics, University of Pennsylvania, Philadelphia, Pennsylvania 19104, United States

^{||}Department of Materials Science and Engineering, North Carolina State University, Raleigh, North Carolina 27695, United States

ABSTRACT: Ultrananocrystalline diamond (UNCD) has become a widely studied material with many potential applications in nanotechnology due to its attractive thermal, mechanical, and chemical properties. While several experimental techniques including Raman spectroscopy have been used to characterize the structural and dynamical properties of UNCD, a detailed understanding of the vibrational dynamics at the atomic level is still lacking. Here, using molecular dynamics simulations, we investigate the structure and dynamics of UNCD to elucidate the role of the grain boundary and interior atoms in detail. Our study considers a UNCD model of 4 nm average grain size, constructed using the Voronoi method. We analyzed the local structure and vibrational properties of the grain boundary and interior atoms. Further, we computed the specific heat of UNCD as a function of temperature from the vibrational spectra. We find that the specific heat of UNCD shows enhancements of approximately 20% over that of single-crystal diamond at 300 K. The excess specific heat in UNCD in comparison to single-crystal diamond is found to be maximum at approximately 350 K. The resolution of the specific heat according to the local structure shows that the excess specific heat arises predominantly from the grain boundaries.



1. INTRODUCTION

There has been recent interest in thin films of polycrystalline diamond, known as ultrananocrystalline diamond (UNCD), that have grain sizes in the range of 2–5 nm.^{1–4} UNCD films can be deposited using microwave plasma chemical vapor deposition (MPCVD) and hot filament chemical vapor deposition (HFCVD) on a variety of substrates. UNCD films have distinct advantages over conventional microcrystalline diamond films for the following reasons: (i) conformal UNCD thin films exhibit smooth surfaces as compared to microcrystalline diamond films and can be grown at complementary metal oxide semiconductor (CMOS) compatible temperatures ($\sim 400^\circ\text{C}$);¹ (ii) physical properties, such as Young's modulus, hardness, and acoustic velocity, remain close to single-crystal diamond despite the high-volume fraction of grain boundaries and the presence of atoms such as hydrogen;^{5,6} and (iii) the small grain size is constant as a function of film thickness, unlike other diamond growth methods which show coarsening.⁷

The impact that the relatively large number of grain boundary atoms in UNCD has on the vibrational properties is less clear. It is well documented that the vibrational spectra of nanocrystalline materials differ from those of materials composed of micrometer and larger crystalline grain sizes. Earlier measurements employing neutron and X-ray inelastic scattering measurements have

revealed that, in general, nanocrystalline materials have an increased number of vibrational modes, primarily in the low-frequency region of the spectra, compared to materials with larger grain sizes. Vibrational properties directly influence several material properties including, for example, the specific heat capacity,⁸ the thermal expansion coefficient, the thermal conductivity (specifically at low temperatures), and the temperature dependence of the elastic constants.⁹ Hence, a detailed understanding of vibrational properties is crucial to gain a complete description of the thermodynamic behavior of UNCD films.

Previous molecular dynamics (MD) simulations have proven to be a very powerful means to gain insight into the atomic level mechanisms that lead to the macroscopic thermal and mechanical properties of amorphous and nanocrystalline materials. For example, Taraskin and Elliott¹⁰ used MD simulations to calculate the specific heat of silica. Similarly, Horbach et al.¹¹ conducted extensive MD simulations on amorphous silica and obtained the temperature-dependent specific heat (C_v) from the vibrational density of states (VDOS). Also, using MD simulations, Wolf et al.¹² reported excess VDOS in the low-frequency region for a

Received: July 3, 2011

Revised: September 20, 2011

Published: September 28, 2011

nanocrystalline model system constructed from an fcc Lennard-Jones crystal. They showed that the presence of grain boundaries leads to additional surface modes and hence an enhancement in the phonon specific heat. Such enhancement of the low-frequency VDOS is also well documented in metallic nanocrystals.^{13,14} Srivastava¹⁵ analyzed phonons in nanocrystals and reported that phonons of certain frequencies are scattered by the boundary of the nanocrystal and that the specific heat depends on the size of the particles.

Theoretical phonon dispersion curves and thermodynamic properties of diamond and graphite based on first-principles calculations have been reported.^{8,16} Similar computational work probing the vibrational properties and specific heat of UNCD, to investigate the role of grain boundary atoms, is yet to be reported. MD simulations were used to study heat transfer across diamond (111) interfaces in model nanostructures.¹⁷ Kebbinski et al. used Monte Carlo simulations to probe the nature of bonding and disorder at diamond grain boundaries.¹⁸ In addition, the thermal conductivity of UNCD models that consisted of columnar grains has been calculated using the Tersoff potential.¹⁹ While these earlier simulations considered somewhat idealized models for interfaces, very recently Remediakis et al.²⁰ investigated the mechanical properties of an UNCD model generated with a Voronoi construction in which grains had random orientations. In particular, they used the Monte Carlo simulations and Tersoff potential to study the effect of grain size on the modulus of UNCD. However, the vibrational properties of UNCD models have not yet been calculated.

In light of the need for addressing the temperature-dependent behavior of vibrational properties in UNCD, we performed MD simulations. The aim of this paper is to investigate the vibrational spectra and specific heat of UNCD as a function of temperature using molecular dynamics (MD) simulations. In this paper, we present a model for UNCD to capture the essential features of its grains and grain boundaries. We report results from MD simulations employing the reactive empirical bond order potential²¹ for calculation of the interatomic forces.

2. COMPUTATIONAL DETAILS

The force field we used in these simulations is the second-generation reactive empirical bond order (REBO-II) potential.²¹ This potential, which is fitted to the experimental values of cohesive energy, lattice parameters, and elastic constants, has been successfully applied in many works concerning a wide variety of carbon systems including diamond,^{22,23} amorphous carbon,²⁴ nanodiamond,²⁵ and nanotubes.^{26,27} This potential function successfully models both sp^2 and sp^3 bonding, depending on the local coordination and degree of conjugation. Classical equations of motion for each atom were numerically integrated using a third-order Nordsieck predictor-corrector algorithm with a time step size 0.5 fs. Prior to calculating the properties, the system was equilibrated at a given temperature using a Langevin thermostat. The NVE ensemble was used for production runs.

Use of an appropriate atomic model with a realistic grain boundary structure is critically important. The structure of grain boundaries in UNCD has received significant attention in recent years as it plays an important role in determining the mechanical, thermal, and electronic properties of UNCD films. Because the grains sizes are extremely small and the grains are randomly oriented,^{28,29} there are numerous possibilities for two crystallographic planes to meet at a grain boundary in UNCD. Thus, in

addition to the fact that carbon can form both sp^2 - and sp^3 -hybridized electronic states, the structure and bonding at the UNCD grain boundaries is complex and not completely known.¹⁸ HRTEM images have provided evidence for randomly oriented crystallites and an atomically sharp grain boundary region.²⁸ A majority of the previous theoretical descriptions of UNCD grain boundaries have, however, limited their studies to "special" grain boundary planes, for example, the high-angle (100) plane or the $\Sigma 13$ twist (100) grain boundary. Recently, however, Remediakis et al.²⁰ as well as Fyta et al.³⁰ studied the mechanical properties of UNCD models that consisted of random grain orientations, also revealing that grain boundaries only a few atomic diameters in width are feasible. We used a Voronoi construction³¹ as detailed below to build our UNCD model.

A set of grain centers was chosen at random but with an average spacing of 4 nm. The region of space closer to a given center than to any other center is filled with atoms in the diamond lattice with a randomly selected crystallographic orientation. While inserting atoms near the Voronoi lines, an insertion is rejected if the atom being inserted is within 2 Å of any existing atom in other grains. This way, no two atoms belonging to two different grains are closer than 2 Å initially (during the course of the simulation they may arrange and rebond to closer spacings). We used a cubic, 3-D periodic simulation box of size $b = 78.556$ Å. Before performing production runs, the system was annealed for 50 ps at 1000 K, allowing unfavorable configurations in the grain boundaries to relax.

The specific heat within the harmonic approximation was calculated by first determining the normalized power spectrum, $g(\nu)$, where ν is the vibrational mode frequency. The power spectrum was determined by Fourier transforming the velocity autocorrelation function (VACF) obtained from the simulations and then normalizing such that $\int g(\nu)d\nu = 1$. It is worthwhile to point out that within a classical harmonic approximation the power spectrum is equivalent to the vibrational density of states (VDOS).³² To calculate the VACF, the velocities of all atoms were sampled every 2 fs time step for 2.5 ps. From the power spectrum, it is straightforward to calculate the temperature dependence of C_v , the specific heat at constant volume, using eq 1.

In this simulation study, we compared the vibrational properties of UNCD with two pure diamond systems: a single-crystal diamond and an isolated nanodiamond (ND) particle. These comparisons are helpful because they provide a basis for understanding how the dynamics of predominantly sp^2 -bonded grain boundary atoms in UNCD alter the vibrational spectrum against an all- sp^3 system with no interfaces or against a nanoparticle, approximately the same size as individual grains in the UNCD model, with surfaces terminated with sp^2 -hybridized atoms. The single-crystal diamond model used in this study consisted of a 3-D periodic cell with $b = 70.89$ Å and 64 000 C atoms in the diamond lattice. The ND particle is of cuboctahedral (CO) shape and consisted of 6232 atoms. The CO particle consists of eight {111} and six {100} facets. The model was cut out from an ideal diamond crystal with a lattice constant of 3.56 Å. Each of these facets is at approximately 40 Å from the center of the cluster.

3. RESULTS AND DISCUSSION

A snapshot of the simulation model is illustrated in Figure 1. It is important to point out that we have not included hydrogen in our model. While experimental data show that grain boundaries contain a small amount of hydrogen atoms (1–4 atom %), we

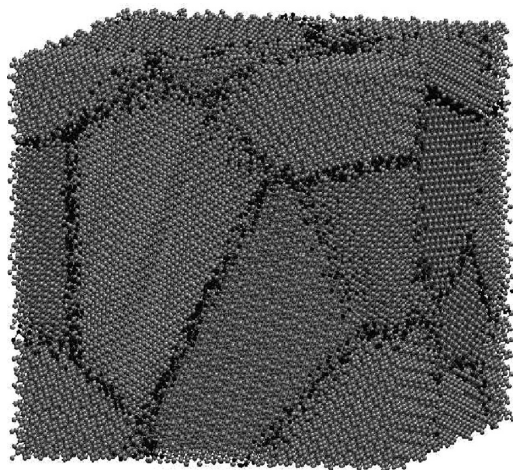


Figure 1. Simulated UNCD model used in this work. The system contains 8 grains and 82 696 atoms and has an average grain diameter of 4 nm. Undercoordinated atoms are colored dark to clearly indicate the grain boundaries.

Table 1. Properties of the Model UNCD System Simulated ($T = 300$ K)

average grain size	4 nm
number of atoms in the system	82 696
density	3.4 g/cm ³
number of grains	8
sp ² content	11.6%
sp ³ content	87.5%
Young's modulus	860 GPa
bulk modulus	382 GPa
average energy/atom	-7.07 eV

excluded them in the present model primarily for the sake of simplicity and to understand the pure carbon case.

The key properties of the UNCD system studied here are tabulated in Table 1. The mechanical properties are characterized in terms of bulk and Young's modulus. The bulk modulus is related to the response of the system to a volume change and is a measure of a material's resistance to hydrostatic tension or compression. The bulk modulus (B) and Young's modulus (E) are calculated by applying small hydrostatic and uniaxial deformations to the material, respectively. We determine the system's response to strain by varying the volume corresponding to the strain value, allowing for relaxation in the atomic positions, calculating the system energy. We find the moduli by fitting parabolas to the energy per unit volume vs strain data; the moduli are equal to the curvature of the parabolas ($1/V)d^2E/d\varepsilon^2$. In the case of Young's modulus, we apply strain along three mutually perpendicular directions, in three separate calculations, and take the average. We obtain values of 382 and 860 GPa for bulk and Young's modulus, respectively. Previously, for example, Remediakis et al.,²⁰ in their simulations using the Tersoff potential, obtained values of 372 and 963 GPa for UNCD models with an average grain size of ~ 4 nm. This discrepancy is partly due to the higher sp² content (11.6%) in our model as compared to 9.6% in their model.

3.1. Radial Distribution Function. To characterize the properties of the UNCD model, we performed various structural

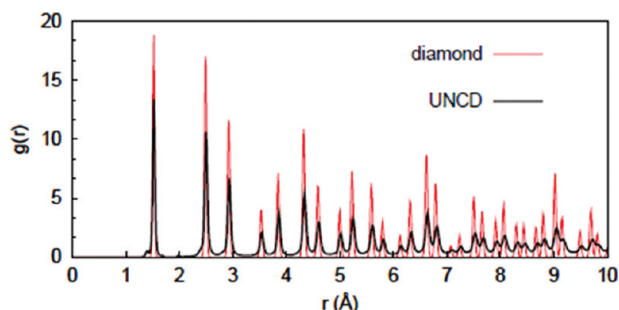


Figure 2. Radial distribution function for single-crystal diamond (black) and UNCD (red) samples at 300 K.

analyses. First, the radial distribution function, which gives the average number of atoms as a function of distance around any given atom, was obtained. It is defined as $g(r) = \langle\langle n(r, \Delta r)\rangle\rangle / (4\pi r^2 \Delta r \rho)$, where $\langle\langle n(r, \Delta r)\rangle\rangle$ is the average number of atoms in a spherical shell of thickness Δr at a distance r from an atom and is an average over all atoms sampled over 10 ps. The number density of atoms ρ is obtained from the mass density of the simulation box. A value of $\Delta r = 0.01$ Å is used. Figure 2 shows the radial distribution functions for single-crystal diamond (solid line) and UNCD (dotted line). The $g(r)$ analysis was obtained for both structures from simulations performed at 300 K. The peak positions in $g(r)$ for the UNCD within the first 1 nm correspond well with the nearest neighbor distances in single-crystal diamond and may be seen as an indication of the structural order corresponding to the diamond lattice inside the grains. The first peak in $g(r)$ of the UNCD system has a small shoulder at ~ 1.41 Å, which corresponds to the bond distance between sp² atoms present in the grain boundaries. The main difference between the distribution functions of the UNCD and the diamond systems is that peaks in the former are of smaller height, have a wider distribution, and diminish significantly at larger distances due to the random grain orientations as well as disorder in the grain boundaries.

3.2. Structure of Grain Boundaries. In Figure 3a we depicted a cross section of the periodic simulation box to show atoms based on their coordination number. The coordination number is calculated by counting all the bonding neighbors of an atom. Two atoms are considered bonded if the distance between them is less than 2 Å, the value corresponding to the minimum between the first two peaks in the radial distribution function. The undercoordinated atoms are shown in darker colors and are mostly confined to very narrow regions where the grains meet. They terminate individual crystallites at the grain boundaries.

To further examine the structure at the atomic level, we classify atoms according to the local crystalline order using the common neighbor analysis (CNA)³³ using the visualization tool OVITO.³⁴ The CNA determines if the local structure around an atom corresponds to the diamond lattice based on the connections it makes to the nearest neighbors. In Figure 3b, the same cross-sectional view of the model UNCD system as Figure 3a is shown with atoms colored based on their local crystalline order. The light-colored atoms are in local diamond crystal order and hence considered core atoms that are 'inside' the grains; all other atoms, colored dark, are considered as belonging to the grain boundaries as they lack local diamond crystal order. The undercoordinated atoms in Figure 3a are confined to a narrower region near the grain boundaries as compared to the atoms that deviate

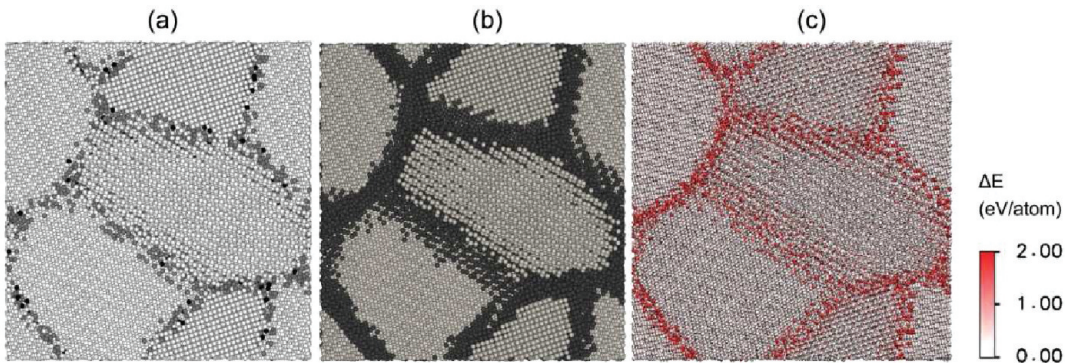


Figure 3. UNCD sample illustrated in Figure 1, with atoms being colored according to (a) coordination number (silver, gray, and black indicate 4-, 3-, and 2-coordinated C atoms, respectively), (b) local crystalline order based on the common neighbor analysis (lighter colored atoms are in diamond crystalline order, and (c) their energy (red color indicates a positive deviation from the average value). Darker colors indicate a higher value of deviation.

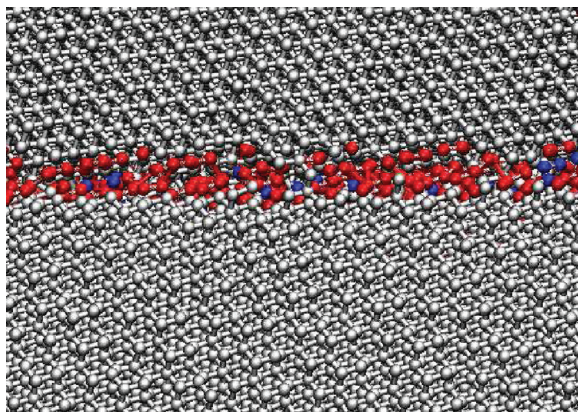


Figure 4. Snapshot from a grain boundary region: 3- and 2-coordinated atoms are colored red and blue, respectively.

from the diamond lattice in Figure 3b. This is because the sp^3 -hybridized atoms near the grain boundaries are often bonded to sp^2 - or sp^1 -hybridized atoms, hence altering their local environment. To determine the width of the GB region we defined a cutoff distance d_{GB} and counted the number of atoms classified as not in a diamond lattice by the CNA. The distance d_{GB} is the distance from an undercoordinated atom; we use this criterion because the undercoordinated atom determines the position of the grain's edge. It was found that 43%, 80%, 90%, and 96% of all atoms classified as not belonging to the core by the CNA are within a distance of $d_{\text{GB}} = 2, 3, 4$, and 5 \AA , respectively, from the nearest undercoordinated atoms. It is important to note that, based on this analysis and the RDF in Figure 2, 80% of all atoms that deviate from a diamond lattice are at most the third nearest neighbor of an undercoordinated atom. Thus, beyond the third neighbor of an undercoordinated atom or within 3.0 \AA from the interface the structure is bulk diamond like.

Atoms are colored based on their potential energy in Figure 3c, with red representing a positive deviation of the potential energy from the mean value. This demonstrates the existence of atoms near the grain boundaries having energy well above the average value, up to 2 eV/atom . A close-up view of a grain boundary is shown in Figure 4, with 3- and 2-coordinated atoms in red and blue, respectively. The grain boundaries are characterized by void regions interspersed with bonds formed between C atoms across the boundary.

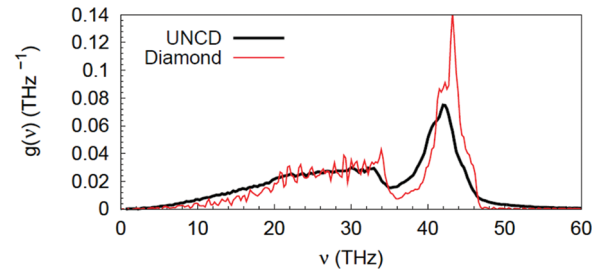


Figure 5. Calculated power spectra for UNCD and single-crystal diamond at $T = 300 \text{ K}$.

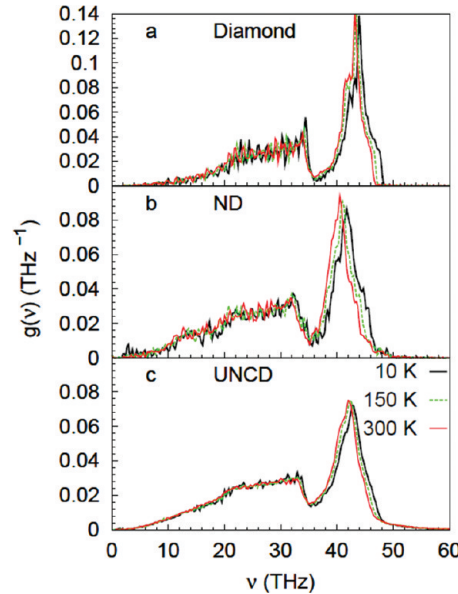


Figure 6. Vibrational spectra at $T = 10, 150$, and 300 K of (a) diamond, (b) cuboctahedral ND particle, and (c) UNCD.

3.3. Vibrational Density of States. In Figure 5, we plotted the computed power spectrum at $T = 300 \text{ K}$ for the UNCD model system and the single-crystal diamond model. Before comparing the spectra for the two model systems, it is important to point out that simulated vibrational spectra have, in general, features shifted to higher energies compared to experiment. For example,

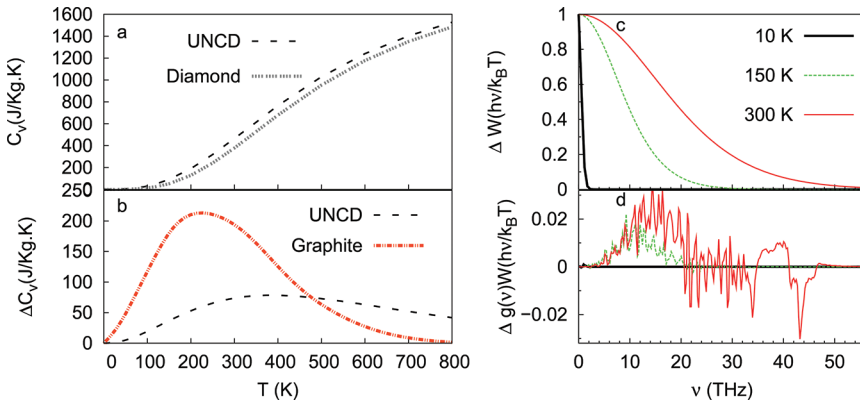


Figure 7. Temperature dependence of (a) the specific heat at constant volume, as calculated from eq 1, for UNCD and diamond models and (b) the excess specific heat of UNCD as compared to single-crystal diamond. For comparison, the excess specific heat for graphite as reported in ref 8 is also plotted. The weighted VDOS, $g(v)W(hv/k_B T)$, is the integrand in the formula of heat capacity (eq 1) and represents the portion of VDOS that contributes to the heat capacity. (c) Weighting factor $W(hv/k_B T)$ and (d) difference in weighted VDOS of UNCD and single-crystal diamond, $g(v)W(hv/k_B T)_{\text{excess}}$, as a function of frequency at $T = 10, 150$, and 300 K.

the simulated spectrum for single-crystal diamond exhibits the main peak corresponding to the optical mode of sp^3 atoms shifted in the direction of higher frequencies (1425 instead of 1258 cm^{-1} found experimentally). This shift lies within the range of deviations observed in previous calculations using bond order potentials.³⁵ Nonetheless, the calculated power spectrum bears reasonably good agreement with the experimental vibrational spectrum of diamond.³⁶ The main feature of the spectrum for single-crystal diamond is a strong peak at ~ 43.2 THz (1425 cm^{-1}) with two shoulders around 41.5 (1384 cm^{-1}) and 45 (1501 cm^{-1}) THz. This peak is followed by a smaller peak at 33.7 THz (1128 cm^{-1}) and a relatively flat region at intermediate frequencies. The overall features of the vibrational spectrum of the UNCD system are similar to that of single-crystal diamond. However, there are significant differences in terms of the shape, height, and position of the main peak. The main peak around 43 THz is red shifted to 42 THz, an effect of phonon confinement which is common to nanocrystalline materials. In addition, this peak is broader and smaller for UNCD. The broad bands in the Raman spectrum of UNCD thin films result from superposition of vibrations related to different structural units.^{28,37} For UNCD, a high-frequency tail extends beyond 47 THz. The high-frequency tail is attributed to strained bonds involving under-coordinated atoms in the grain boundaries that have enhanced force constants.

In Figure 6 we show the power spectra for temperatures $T = 10, 150$, and 300 K for (a) diamond, (b) ND, and (c) UNCD systems. From the temperature dependence of the spectra, we see that the main change in $g(v)$ occurs at high frequencies in that, with increasing temperature, the height of the main peak increases and its location shifts to lower frequencies, i.e., the corresponding vibrations become slower. At intermediate and low frequencies, the effect of temperature on the vibrational spectrum is mainly to smoothen out the finely spaced features. The spectra of the ND particle bears similarities to the UNCD model in terms of the high-frequency tail (beyond 50 THz) due to the undercoordinated atoms at the surface as well as enhancements in the low–medium-frequency region. Because the shape of the ND particle is well defined as compared to the crystallites in the UNCD model, the spectral features are less broadened as compared to UNCD.

3.4. Specific Heat and Debye Temperature. To study the effect of temperature on the specific heat of UNCD, the phonon specific heats of UNCD and diamond are computed from the vibrational spectra using the following equation

$$C_v = \frac{h^2}{k_B T^2} \int_0^\infty \frac{\nu^2 \exp(h\nu/k_B T)}{(\exp(h\nu/k_B T) - 1)^2} g(\nu) d\nu \quad (1)$$

The plot in Figure 7a shows the specific heat of UNCD and single-crystal diamond as a function of temperature. We note that our computed value of the C_v of diamond is lower than that of the experimental values, for example, the computed C_v is 380 J/kg·K at 300 K as compared to the experimental value of 502 J/kg·K. This discrepancy is due to many factors including (i) the absence of defects such as vacancies, impurities, and isotopes in our model and (ii) the interatomic potential. For example, previous calculations of the C_v of diamond employing the REBO-II have reported similar deviations in the computed C_v from experimental values.³⁸

The specific heat of UNCD is enhanced as compared to single-crystal diamond over the whole range of the temperature we considered. The excess specific heat as a function of temperature is plotted in Figure 7b. For comparison, the excess specific heat of graphite compared to diamond as obtained from ref 8 is also plotted. The excess specific heat of UNCD goes through a maximum value at approximately 350 K and is approximately 15% greater than single-crystal diamond. To illustrate how different frequency regions in the VDOS of UNCD contribute to the excess density of states, we analyzed the weighted VDOS given by the product of $g(v)$ and $W(hv/k_B T) = (hv/k_B T)^2 \exp(hv/k_B T) / [\exp(hv/k_B T) - 1]^2$. The weighting factor, $W(hv/k_B T)$, which represents the proportion of the vibrational states that can be excited and contributes to the heat capacity at a given temperature, is plotted for different temperatures in Figure 7c. In Figure 7d, the excess in weighted VDOS, calculated as the difference between $g(v)W(hv/k_B T)$ of UNCD and diamond at $T = 10, 150$, and 300 K is plotted. From the plots it can be inferred that at low temperature ($T = 10$ K), only low-frequency states (< 5 THz) can contribute to the excess heat capacity. At higher temperatures ($T = 150$ and 300 K), the majority of the contribution to excess specific heat comes from vibrational states that lie between 5 and 20 THz. The enhanced contribution of

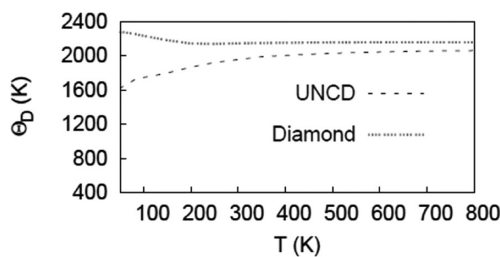


Figure 8. Debye temperature Θ_D as a function of temperature for UNCD and diamond. Θ_D was extracted from eq 2 by plugging in the simulated C_v value.

low–medium-frequency acoustic phonons to heat capacity explains the noticeable deviations between the C_v of UNCD and diamond.

The relative importance of the contribution from frequencies < 20 THz occurs mostly at low temperatures. As the temperature increases the relative contribution of excess states in the low–medium-frequency region in UNCD becomes less important. Therefore, the excess C_v goes through a maximum around 350 K. In comparison, the maximal excess for bulk graphite in relation to bulk single-crystal diamond (Figure 7b) occurs around 200 K. Note that in UNCD excess specific heat is due to the contributions from atoms at grain boundaries (undercoordinated sp^2 and sp^1 atoms, sp^3 atoms bonded to undercoordinated atoms, or sp^3 atoms very close to grain boundaries) which have slightly different bonding energies as opposed to the perfect order of sp^3 -bonded diamond or sp^2 -bonded graphite. We note that the sharp sp^3 features of single-crystal diamond or sp^2 -bonded graphite visible in the VDOS are broadened by the different energy landscapes due to the disorder at the grain boundaries. This broadening of the VDOS features results in excess specific heat.

Our results are in good qualitative agreement with findings of previous theoretical studies of other nanocrystalline systems. For example, specific heat calculations of nanocrystalline Cu show that specific heat is enhanced compared with single-crystal Cu and the excess goes through a maximum at a temperature around 50 K.¹³ The fact that UNCD has a higher temperature where the excess goes through a maximum is a reflection of its stronger, more energetic bonds and the need to reach higher temperatures to excite the relevant modes.

We now turn to the Debye temperature (Θ_D) of UNCD. It is related to the Debye frequency ν_D as $\Theta_D = h\nu_D/k_B$ and within the harmonic approximation relates to the stiffness of the material. From the simulated C_v vs temperature behavior one can calculate the Debye temperature as a function of temperature. In the Debye model, the specific heat is calculated as follows³⁹

$$C_v = 9R \left(\frac{T}{\Theta_D} \right)^3 \int_0^{\Theta_D/T} \frac{x^4 e^x}{(e^x - 1)^2} dx \quad (2)$$

Here, $x = h\nu/k_B T$ and R is the gas constant. The Debye temperature at a given temperature was determined by fitting the simulated C_v to that from eq 2. We plotted the Debye temperatures for UNCD and diamond models as a function of temperature in Figure 8. It is important to note that the calculated Debye temperature is the theoretical equivalent of the calorimetric Debye temperature in experiments, i.e., this is the Debye temperature that is fit to the calculated (equivalent of the experimentally measured value) C_v and both acoustic and

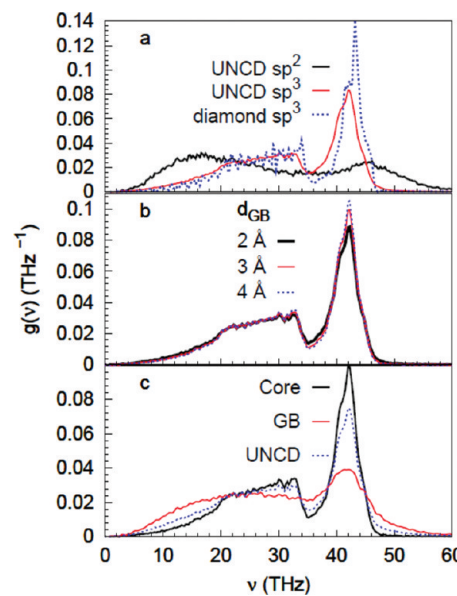


Figure 9. (a) Normalized partial vibrational spectra for sp^2 - and sp^3 -hybridized atoms in UNCD. For comparison, the vibrational spectrum of single-crystal diamond is also included. (b) Normalized partial vibrational spectra of the core atoms defined using values of d_{GB} = 2, 3, and 4 Å. (c) Normalized partial vibrational spectra of the core and GB atoms for d_{GB} = 3 Å. The total spectrum (UNCD system) is also shown for comparison. $T = 300$ K in all cases.

optical phonons contribute to it. This value is different than the elastic Debye temperature which is estimated from the sound velocity (in turn derived from the Young's modulus and density). The Debye temperature of diamond is overestimated in our calculations¹⁶ because the simulated C_v values in our work is lower than the experimental values as discussed previously. However, the relative values of diamond and UNCD models can provide important information about the stiffness of the material. The Debye temperature of UNCD is approximately 8% lower than that of diamond at 300 K. The softening of UNCD can be explained on the basis of grain boundary atoms leading to an enhancement of soft modes in the vibrational spectra as compared to diamond.

3.5. Contribution of Grain Boundary atoms. To determine the influence of grain boundary atoms on the vibrational properties of UNCD we decomposed the spectra into contributions from GB atoms and interior atoms. We use two different analyses to distinguish contributions from GB and interior atoms. In the first analysis, we decompose the spectra into contributions from sp^1 , sp^2 , and sp^3 -hybridized atoms. Because all the sp^1 and sp^2 atoms are located in the GB this is a very useful analysis to gain insight into the dynamics of undercoordinated atoms in the GB. The results of these calculations are shown in Figure 9a. In the plot, we compare the normalized partial vibrational spectra of sp^2 -hybridized and sp^3 -hybridized atoms at 300 K. For reference, the vibrational spectrum of single-crystal diamond (all sp^3 atoms) is also plotted. The partial spectra of sp^2 atoms are mostly disordered. Because of the disordered nature of the grain boundaries the $g(\nu)$ better resembles sp^2 atoms in amorphous carbon⁴⁰ than sp^2 atoms in graphite.¹⁶ In contrast, the vibrational spectrum of atoms inside the grains (sp^3) is more structured and depicts signatures of sp^3 carbon atoms in diamond. Much of the difference between $g(\nu)$ of sp^3 atoms in UNCD and that in diamond is

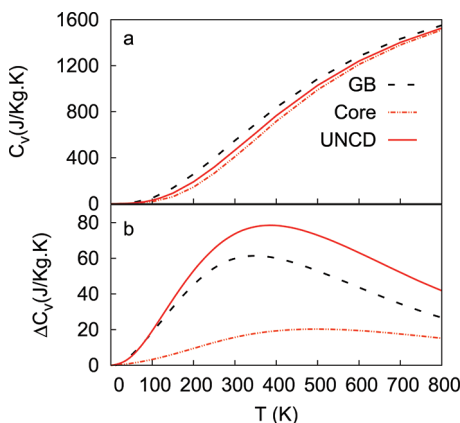


Figure 10. (a) C_v of GB and core atoms as a function of temperature. C_v of the UNCD system as a whole is plotted for reference. (b) Excess specific heat of UNCD with respect to single-crystal diamond and its break up into contributions from GB and core atoms.

because in UNCD a significant fraction of sp^3 atoms are near grain boundaries and connected to sp^2 atoms. It is well known that next nearest neighbor effects modify the local density of states. Distortions of the bonding geometry of the sp^3 atoms near the grain boundaries modify the vibrational states and may account for the changes observed in the low-frequency region. We will probe this in the second analysis. To estimate the relative contribution of sp^2 and sp^3 atoms to the total specific heat we used the following expression to describe the total specific heat

$$C_v = x^{sp^1} C_v^{sp^1} + x^{sp^2} C_v^{sp^2} + x^{sp^3} C_v^{sp^3} \quad (3)$$

Here, x^y and C_v^y are the fraction of atoms and specific heat derived from the partial vibrational spectrum, respectively, for species y . In this analysis the total specific heat is calculated as a sum of contributions of different species.⁴¹ At $T = 300$ K, the sp^2 - and sp^3 -coordinate atoms contributed 16% and 82%, respectively, to the total specific heat.

In the second analysis, we define GB atoms as all sp^1 and sp^2 atoms and those sp^3 atoms that are located within a distance d_{GB} of the undercoordinated atoms. The core atoms are defined as those sp^3 atoms that are at a distance greater than d_{GB} from the nearest undercoordinated atom. First, we probe the distance to which the effect of the grain boundaries is reflected in terms of the vibrational properties of the atoms by calculating the partial spectra of the interior atoms for different values of d_{GB} . In Figure 9b we show the normalized partial spectra at 300 K for interior atoms defined using values of $d_{GB} = 2, 3$, and 4 \AA . As d_{GB} increases the size of the core reduces and more atoms close to the GB will be eliminated. This is reflected in the spectra, as d_{GB} is increased from 2 to 4 \AA the spectra of the core atoms become more defined with an increase in the intensity of the sp^3 peak at 42 THz. It is important to note that the change in the intensity of the main peak is more pronounced when d_{GB} is increased from 2 to 3 \AA as compared to when it is increased from 3 to 4 \AA . Eliminating more atoms near the GB by increasing the d_{GB} to 5 and 6 \AA did not cause a considerable change in the spectra of the core atoms (not shown here), indicating that a choice $d_{GB} = 3 \text{ \AA}$ is suitable in defining the GB region. This is consistent with the results of the CNA presented previously which showed that 80% of all the disordered sp^3 atoms are accounted for in the GB region with $d_{GB} = 3 \text{ \AA}$. On the basis of this analysis we chose a GB region

with $d_{GB} = 3 \text{ \AA}$ in our analysis of the partial contributions of GB and core atoms. In Figure 9c we show normalized partial spectra of GB and core atoms at 300 K. For comparison the total spectrum of the UNCD system is also plotted. The spectrum of GB atoms is clearly disordered as it shows signatures of both undercoordinated and sp^3 atoms. The optical peak due to sp^3 atoms in the core region is red shifted to 42 THz as compared to single-crystalline diamond (43.2 THz) due to the phonon confinement effect. On the basis of the comparison of the spectra of GB and core atoms with the total spectra of the UNCD system, the enhancement of the acoustical modes at lower frequency can be directly attributed to the GB atoms.

Now we analyze the specific heat of GB and core atoms as a function of temperature. In Figure 10a the specific heat of GB and core atoms are plotted as a function of temperature along with that of the UNCD system as a whole. The C_v of the UNCD system lies between that of the GB and core atoms. The C_v of the UNCD system can be represented by the sum of contributions from the GB and the core part as follows

$$C_v = x^{GB} C_v^{GB} + x^{Core} C_v^{Core} \quad (4)$$

Here, x^y and C_v^y are the fraction of atoms and specific heat derived from the partial vibrational spectrum, respectively, for species y . For example, based on partial vibrational spectra analysis, GB and core atoms contribute 48% and 52%, respectively, to the C_v of UNCD at 300 K. We then calculate the contributions of the GB and the core atoms to the excess C_v of UNCD with respect to diamond as $\Delta C_v^{GB} = X^{GB} (C_v^{GB} - C_v^{Dia})$ and $\Delta C_v^{Core} = X^{Core} (C_v^{Core} - C_v^{Dia})$, respectively. The fraction of GB atoms for $d_{GB} = 3 \text{ \AA}$ was found to be 0.4. From the plots of these two excess contributions and their sum (the total excess for the UNCD system) in Figure 10b it is readily seen that the GB atoms are the strongest contributors to the total excess from 0 to 600 K, after which the two contributions become comparable.

We can generalize our findings to estimate the C_v of a UNCD system for a given temperature and grain size if one assumes that the thickness and the structure of the GB region are not dependent on the grain size, and thus, the C_v of GB and core atoms are constants. Under this assumption, only the fractions of GB (x^{GB}) and core atoms (x^{Core}) change with the grain size and an analysis similar to the one in ref 41 may be used to estimate these quantities. Finally, eq 4 can be used to calculate the C_v of UNCD as a linear combination of the two parts for any given grain size.

4. CONCLUSIONS

We presented results from MD simulations of UNCD in which we used the reactive empirical bond order potential to model the interactions. We used the velocity autocorrelation function obtained from the simulations to calculate an effective density of states $g(\nu)$.

Our analysis of the vibrational properties of UNCD leads us to conclude that the vibrational density of states exhibit enhancements that arise from atoms at and near the grain boundaries. This is reflected in the calculated phonon specific heat of UNCD, which is approximately 20% higher than single-crystal diamond at room temperature. Because these enhancements are in the 5–20 THz frequency region, the excess C_v as a function of temperature goes through a maximum value at approximately 350 K, above which the low–medium-frequency enhancements contribute less and less to specific heat.

We classified atoms based on their local structure and vibrational dynamics into GB and core atoms. The GB region extends $\sim 3 \text{ \AA}$ into the grains on each side of the interface and consists of both the undercoordinated sp^1 and sp^2 atoms and the sp^3 atoms that deviate from bulk diamond structure. Our analysis of partial spectra shows that the enhancements are primarily due to these GB atoms which are reflected in the excess specific heat of UNCD as compared to single-crystal diamond.

The enhancement of acoustic modes leads to a reduction in the Debye temperature of UNCD compared to single-crystal diamond, which is a measure of the stiffness of the material. We find that the Debye temperature of UNCD is $\sim 8\%$ lower than that of diamond at 300 K.

It is important, however, to note that our results are based on just one model for the UNCD system, and actual UNCD films may consist of grain boundary structures that are more diverse in terms of grain boundary angles and interface structures. Nonetheless, the work provides a deeper understanding of the vibrational properties of UNCD and especially the differences between UNCD and single-crystal diamond. For future work, it would be desirable to investigate the influence of impurity atoms such as hydrogen present in the grain boundaries on the vibrational properties of atoms close to grain boundaries and the corresponding effects that it has on thermal and mechanical properties.

AUTHOR INFORMATION

Corresponding Author

*E-mail: shashi.adiga@gmail.com.

ACKNOWLEDGMENT

Use of computer resources from the Computational Center for Nanotechnology Innovations (CCNI) at Rensselaer Polytechnic Institute (RPI) is gratefully acknowledged. V.P.A. and R.W.C. are supported by the Nano/Bio Interface Center through the National Science Foundation NSEC (DMR08-32802). D.W.B. is supported by the Office of Naval Research through contract N000141-01-01-6-8.

REFERENCES

- Krauss, A. R.; Auciello, O.; Gruen, D. M.; Jayatissa, A.; Sumant, A.; Tucek, J.; Mancini, D. C.; Moldovan, N.; Erdemir, A.; Ersoy, D.; et al. Ultrananocrystalline diamond thin films for MEMS and moving mechanical assembly devices. *Diamond Relat. Mater.* **2001**, *10*, 1952–1961.
- Gruen, D. M. Nanocrystalline Diamond Films. *Ann. Rev. Mater. Sci.* **1999**, *29*, 211–259.
- Sumant, A. V.; Auciello, O.; Carpick, R. W.; Srinivasan, S.; Butler, J. E. Ultrananocrystalline and nanocrystalline diamond thin films for MEMS/NEMS Applications. *MRS Bull.* **2010**, *35*, 281–288.
- Fletcher, P. C.; Felts, J. R.; Dai, Z.; Jacobs, T. D.; Zeng, H.; Lee, W.; Sheehan, P. E.; Carlisle, J. A.; Carpick, R. W.; King, W. P. Wear-Resistant Diamond Nanoprobe Tips with Integrated Silicon Heater for Tip-Based Nanomanufacturing. *ACS Nano* **2010**, *4* (6), 3338–3344.
- Adiga, V. P.; Sumant, A. V.; Suresh, S.; Gudeman, C.; Auciello, O.; Carlisle, J. A.; Carpick, R. W. Mechanical Stiffness and Dissipation in Ultrananocrystalline Diamond Microresonators. *Phys. Rev. B* **2009**, *79* (245403), 1–8.
- Liu, C.; Xiao, X. C.; Wang, J.; Shi, B.; Adiga, V. P.; Carpick, R. W.; Carlisle, J. A.; Auciello, O. Dielectric Properties of Hydrogen-incorporated Chemical Vapor Deposited Diamond Thin Films. *J. Appl. Phys.* **2007**, *102* (074115), 1–7.
- Qin, L. C.; Zhou, D.; Krauss, A. R.; Gruen, D. M. TEM Characterization of Nanodiamond Thin Films. *Nanostruct. Mater.* **1998**, *10*, 649–660.
- Mounet, N.; Marzari, N. First-Principles Determination of the Structural, Vibrational and Thermodynamic Properties of Diamond, Graphite, and Derivatives. *Phys. Rev. B* **2005**, *71* (205214), 1–14.
- Anderson, O. L. *Equations of State for Solids in Geophysics and Ceramic Science*, 1st ed.; Oxford University Press: New York, 1995.
- Taraskin, S. N.; Elliott, S. R. Nature of Vibrational Excitations in Vitreous Silica. *Phys. Rev. B* **1997**, *56*, 8605–8622.
- Horbach, J.; Kob, W.; Binder, K. Specific Heat of Amorphous Silica within the Harmonic Approximation. *J. Phys. Chem. B* **1999**, *103*, 4104–4108.
- Wolf, D.; Wang, J.; Phillpot, S. R.; Gleiter, H. Phonon-induced Anomalous Specific Heat of a Nanocrystalline Model Material by Computer Simulation. *Phys. Rev. Lett.* **1995**, *74*, 4686–4689.
- Meyer, R.; Lewis, L. J.; Prakash, S.; Entel, P. Vibrational Properties of Nanoscale Materials: from Nanoparticles to Nanocrystalline Materials. *Phys. Rev. B* **2003**, *68* (104303), 1–12.
- Derlet, P. M.; Meyer, R.; Lewis, L. J.; Stuhr, U.; Van Wykkenhoven, H. Low-Frequency Vibrational Properties of Nanocrystalline Materials. *Phys. Rev. Lett.* **2001**, *87* (205501), 1–4.
- Shrivastava, K. N. Specific Heat of Nanocrystals. *Nano Lett.* **2002**, *2*, 21–24.
- Tohei, T.; Kuwabara, A.; Oba, F.; Tanaka, I. Debye Temperature and Stiffness of Carbon and Boron Nitride Polymorphs from First Principles Calculations. *Phys. Rev. B* **2006**, *73* (064304), 1–7.
- Mozyar, O. A.; Hase, W. L. Dynamics and Kinetics of Heat Transfer at the Interface of Model Diamond {111} Nanosurfaces. *J. Phys. Chem. A* **2006**, *110*, 526–536.
- Kebinski, P.; Wolf, D.; Phillpot, S. R.; Gleiter, H. Role of bonding and coordination in the atomic structure and energy of diamond and silicon grain boundaries. *J. Mater. Res.* **1998**, *13*, 2077–2100.
- Angadi, M. A.; Watababe, T.; Bodapati, A.; Xiao, X.; Auciello, O.; et al. Thermal transport and grain boundary conductance in ultrananocrystalline diamond thin films. *J. Appl. Phys.* **2006**, *99* (114301), 1–6.
- Remedakis, I. N.; Kopidakis, G.; Kelires, P. C. Softening of ultra-nanocrystalline diamond at low grain sizes. *Acta Mater.* **2008**, *56*, 5340–5344.
- Brenner, D. W.; Shenderova, O. A.; Harrison, J. A.; Stuart, S. J.; Ni, B.; Sinnott, S. B. A second-generation reactive empirical bond order (REBO) potential energy expression for hydrocarbons. *J. Phys.: Condens. Matter* **2002**, *14*, 783–802.
- Shenderova, O. A.; Brenner, D. W.; Omelchenko, A.; Su, X.; Yang, L. H. Atomistic Modeling of the Fracture of Polycrystalline Diamond. *Phys. Rev. B* **2000**, *61*, 3877–3888.
- Gao, G.; Workum, K. V.; Schall, J. D.; Harrison, J. A. Elastic Constants of Diamond from Molecular Dynamics Simulations. *J. Phys.: Condens. Matter* **2006**, *18*, S1737–S1750.
- Gao, G. T.; Mikulski, P. T.; Chateauneuf, G. M.; Harrison, J. A. The Effects of Film Structure and Surface Hydrogen on the Properties of Amorphous Carbon Films. *J. Phys. Chem. B* **2003**, *107*, 11082–11090.
- Adiga, S. P.; Curtiss, L. A.; Gruen, D. M. In *Nanodiamonds: Applications in Biology and Nanoscale Medicine*, 1st ed.; Ho, D., Ed.; Springer: New York, 2010.
- Garg, A.; Sinnott, S. B. Effect of Chemical Functionalization on the Mechanical Properties of Carbon Nanotubes. *Chem. Phys. Lett.* **1998**, *295*, 273–278.
- Ni, B.; Sinnott, S. B.; Mikulski, P.; Harrison, J. A. Compression of Carbon Nanotubes Filled with C_{60} , CH_4 , or Ne: Predictions from Molecular Dynamics Simulations. *Phys. Rev. Lett.* **2002**, *88* (205505), 1–4.
- Birrell, J.; Carlisle, J. A.; Auciello, O.; Gruen, D. M.; Gibson, J. M. Morphology and Electronic Structure of Nitrogen-doped Ultrananocrystalline Diamond. *App. Phys. Lett.* **2002**, *81*, 2235–2237.
- May, P. W.; Mankelevich, Y. A. From Ultrananocrystalline Diamond to Single Crystal Diamond Growth in Hot Filament and Microwave Plasma-Enhanced CVD Reactors: a Unified Model for Growth Rates and Grain Sizes. *J. Phys. Chem. C* **2008**, *112*, 12432–12441.

- (30) Fyta, M.; Hadjisavvas, G.; Kelires, P. Probing the sp^2 Dependence of Elastic Moduli in Ultrahard Diamond Films. *Diamond Relat. Mater.* **2007**, *16*, 1643–1647.
- (31) Schiøtz, J.; Di Tolla, F. D.; Jacobsen, K. W. Softening of Nanocrystalline Metals at Very Small Grain Sizes. *Nature* **1998**, *391*, 561–563.
- (32) Dicky, J. M.; Paskin, A. Computer Simulation of the Lattice Dynamics of Solids. *Phys. Rev.* **1969**, *188*, 1407–1418.
- (33) Honeycutt, J. D.; Anderson, H. C. Molecular Dynamics Study of Melting and Freezing of Small Lennard-Jones Clusters. *J. Phys. Chem.* **1987**, *91*, 4950–4963.
- (34) Stukowski, A. Visualization and Analysis of Atomistic Simulation Data with OVITO—the Open Visualization Tool. *Modelling Simul. Mater. Sci. Eng.* **2010**, *18* (015012), 1–7.
- (35) Rosenblum, I.; Adler, J.; Brandon, S. Calculation of Thermal Properties of Diamond from Simulated Phonon Spectra. *Comput. Mater. Sci.* **1998**, *12*, 9–25.
- (36) Walker, J. Optical Absorption and Luminescence in Diamond. *Rep. Prog. Phys.* **1987**, *42*, 1605.
- (37) Birrell, J.; Gerbi, J. E.; Auciello, O.; Gibson, J. M.; Johnson, J.; Carlisle, J. A. Interpretation of the Raman Spectra of Ultrananocrystalline Diamond. *Dia. Rel. Mat.* **2005**, *14*, 86–92.
- (38) Jiang, H.; Huang, Y.; Hwang, K. C. A Finite-Temperature Continuum Theory Based on Interatomic Potentials. *J. Eng. Mater. Technol.* **2005**, *127*, 408–416.
- (39) McQuarrie, D. A. *Statistical Mechanics*; Harper Collins: New York, 1976.
- (40) Wang, C. Z.; Ho, K. M. Structure, dynamics, and electronic properties of diamondlike amorphous carbon. *Phys. Rev. Lett.* **1993**, *71*, 1184–1187.
- (41) Zhang, H.; Banfield, J. F. A Model for Exploring Particle Size and Temperature Dependence of Excess Heat Capacities of Nanocrystalline Substances. *Nano Struct. Mater.* **1998**, *10*, 185–194.